Reducing observer metamerism in wide-gamut multiprimary displays

David Long, Mark D Fairchild
Program of Color Science, Rochester Institute of Technology

ABSTRACT

Emerging electronic display technologies for cinema and television such as LED, OLED, laser and quantum dot are permitting greatly enhanced color gamuts via increasingly narrow-band primary emission spectra. A recent standard adopted for Ultra High Definition television, ITU-R Rec. 2020, promotes RGB primary chromaticities coincident with the spectral locus. As displays trend towards larger gamuts in the traditional 3-primary design, variability in human color sensing is exacerbated. Metameric matches to aim stimuli for one particular observer may yield a notable color mismatch for others, even if all observers are members of a color-normal population. Multiprimary design paradigms may hold value for simultaneously enhancing color gamut and reducing observer metamerism. By carefully selecting primary spectra in systems employing more than 3 emission channels, intentional metameric performance can be controlled. At Rochester Institute of Technology, a prototype multiprimary display has been simulated to minimize observer metamerism and observer variability according to custom indices derived from emerging models for human color vision. The constructed display is further being implemented in observer experiments to validate practical performance and confirm these vision and metamerism models.

Keywords: observer metamerism, observer variability, multispectral imaging, multiprimary display, cinema

1. INTRODUCTION

For over 100 years, the cinema has afforded filmmakers the opportunity to share intentional visual experiences with moviegoers, the result of their mastering photographic technologies to render creative efforts on screens both big and small. The model of distribution for these artistic endeavors has been mostly reliable and predictable. Color stimuli generated on screen during a movie's mastering can survive to the ultimate audience with little distortion in presentation and interpretation. In the era of film capture and projection, filmmakers mastered the workflows of absorptive dye technology, learning film's palette and shaping each frame through lighting, art direction and optical printing to yield the desired impact. For traditional electronic distribution via video broadcast, the additive color technologies of CRT phosphors together with international standards for television color management proved robust to the visual sensitivities of most viewers. However, reproduction of color in cinematic reproduction has always been a well-crafted illusion of the human visual system.

More than 150 years after Maxwell first proposed the theory of trichromatic color reproduction, all practical motion-imaging systems continue to rely on metamerism wherein a particular integrated stimulation of the three cone types found on the human retina is sufficient to reproduce the sensation of color of any real object, regardless of higher order spectral composition. Manufacturers and content producers have mastered these techniques in both additive and subtractive color reproduction models, relying on agreed upon standard observer models such as are available from the CIE[1]. This simplified treatment, though effective, is necessarily restrictive in light of emerging trends including the introduction of wide-gamut display technologies.

Concerns in the trichromatic reproduction model are emerging in the form of variability in human color vision. Controlled metameric matches of color within the display for a single observer may prove not to be matches for another observer with slightly different color-matching functions (CMFs) or may prove inconsistent even for single observers as they age[2]. Dye-based film systems and phosphor-based CRT displays are generally forgiving in the metamerism illusion across disparate observers. Broad spectral representation in each colorant limits the chance for quantal integration differences within the cones amongst a diverse population. But evolving technologies for both large and small screens employ new physics with LED, OLED, laser and quantum dot illumination systems. These displays are decidedly more narrow-band in their spectral composition, an intentional design feature which influences reproducible color gamut. The next generation of Ultra High Definition televisions will conform to ITU-R Rec. 2020 standards, employing

monochromatic RGB primaries suited to maximizing color volume in a 3-channel paradigm. Previous research confirms that spectrally selective primary sets necessary for expanding color gamut exacerbate observer variability[3]. In related work, the Society of Motion Picture and Television Engineers is exploring alternatives to standard observer colorimetry for calibrating newer video mastering displays employing these same physics. This stems from user experience where visual white point calibrations made between flat-panel displays and reference CRT displays are inconsistent with calibrations made alternatively by standard colorimeters employing a single observer CMF[4,5].

Multispectral imaging systems offer options for co-optimization of increased palette and reduced observer variability. In the ideal case, narrow-bandwidth, high-spectral-resolution systems would be conceived to accomplish the goals of controllable spectral capture and reproduction of target stimuli. By combining near-monochromatic characteristics at a high sample rate across the visible electromagnetic spectrum, many sufficiently complex stimuli could be rigorously rendered. However, these solutions require optically-complex, processing-intensive systems that often compromise spatial quality for spectral precision. The present research seeks to confirm that an abridged primary display system is capable of minimizing observer metamerism while delivering enhanced color gamut.

The design of such a system, though, must be deliberate, assessed against meaningful objective criteria for color reproduction, metamerism reduction and spectral gamut. Recent work at Rochester Institute of Technology (RIT) has focused on three critical components of the multispectral system ecosystem: 1) Observer color-matching-function demographics, 2) observer variability index definitions and 3) abridged multispectral display optimization. Previous publications outline many of the results of objectives 1 and 2[6,7,8,9]. Here, summary of efforts to build and test a prototype system are provided. The intended purpose of the RIT multispectral display is to confirm current understanding of variabilities amongst real observers and to provide evidence for potential in metamerism reduction versus emerging cinema display technologies.

2. DESIGN METHODOLOGY

The starting objective for design of the RIT multi-primary display (MPD) was to deliver meaningfully reduced observer variability versus traditional 3-channel RGB systems. The MPD display was modeled as a 2-part optical projection system comprising a wide-band illumination source and individual transmission filters defining distinct color channels. All channels utilized a common source so as to permit consistency in either time-multiplexed or space-multiplexed prototype configurations. Candidate filter spectra were originally simulated via parametric optimization as opposed to being restricted to a heuristic selection from a set of available commercial color filters. The final design was implemented using materials then that performed most closely to the resultant computational models. In this manner, deficiencies in available filter sets could be quantified versus optimized results. To keep the mathematics simple in the constrained computational optimization, a generalized Gaussian transmission profile, $\boldsymbol{T(\lambda)}$, was modeled for each potential primary filter, equation 1. The peak transmission fraction of all candidates was normalized to 1.0 and no accounting for system white balance was otherwise enforced. Subsequent assessments of the MPD prototype were performed via absolute radiometric models and thus no color management against traditional normalized white was required.

$$T(\lambda) = \frac{1}{\sigma\sqrt{2\pi}} exp\left[-\frac{(\lambda-\mu)^2}{2\sigma^2}\right] \quad (1)$$

For the design, candidate transmission filters were illuminated using one of two measured source spectra common in cinema applications and generally available for prototype construction, one a typical large-venue xenon arc lamp and the other a consumer-grade mercury arc UHP lamp, see Figure 1 for spectra. Thus the modeled MPD primaries in each channel represent the absolute spectral concatenation of the illumination source and the transmission profile of the simulated Gaussian filter. Across *N* total primaries for the display system, the transmission profiles were varied in both peak transmission wavelength, $\boldsymbol{\mu}$, and profile-width, $\boldsymbol{\sigma}$, in order to achieve cost function minimization. The majority of simulations were executed with Matlab's *fmincon* optimization tool. Additional permutations investigated for the system design included the number of primaries (*N*=3 through 8), the starting guess for Gaussian parameters and the spectral

domain permitted for iteration of each primary's characteristics (each primary having it's peak wavelength constrained to a window of wavelengths versus permitting any monotonic array of peak wavelengths for the *N* primaries between constrained spectral endpoints of 400 and 700nm).

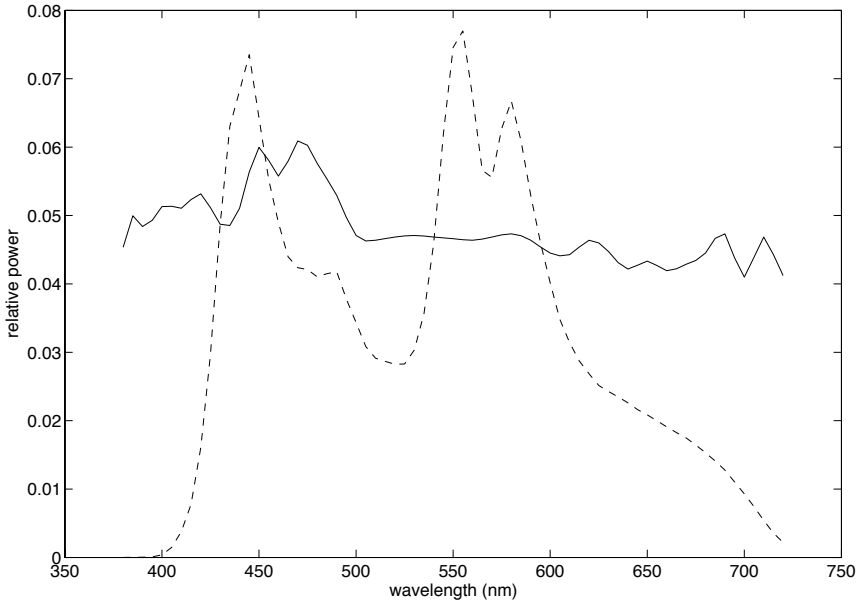

Figure 1. Projector illuminant candidates for the RIT MPD: xenon (solid) and mercury arc UHP (dashed)

The cost function objective for the primary parameter optimizations was minimized observer metamerism in the MPD display's reproduction of a set of *a priori* reference spectra. Specifically, a training/verification strategy was employed where only one candidate collection of spectra was chosen for inclusion in the optimization routine. Additional unique spectra were then used with the optimization results to verify model quality. A collection of six different candidate reflective spectra sets were investigated and compared for training the MPD design, see Table 1. The two MacBeth Color Checkers represent popular color calibration tools used for image capture and which are widely available for practical experimentation. The Kodak/AMPAS set is a collection of 190 spectra determined by Kodak to deliver superior statistical representation of typical surface colors encountered in traditional photography. It is also the spectra set currently recommended by the Academy of Motion Picture Arts and Sciences for color management research. The high metamerism colors were similarly derived from Kodak research as a subset of surface colors with particularly high metamerism failure in traditional photographic applications. Munsell spectra were measured from a sample matte Munsell Book of Colors. Finally, the Standard Object Colour Spectra (SOCS) database is a compilation of many other spectra sets and includes skintones, textiles, flowers, leaves, paints, photographic materials and printing inks/pigments. There are certainly other high quality candidate sets which were not included but may be investigated in future work[10].

Table 1. Reflectance patchsets considered in MPD design optimization

1) MacBeth Color Checker (24 samples)
2) MacBeth Color Checker DC (240 samples)
3) US Patent No. 5,582,961 "Kodak/AMPAS" test spectra (190 samples)
4) Munsell sample spectra (1269 samples)
5) select high metamerism color set (65 samples)
6) SOCS[11] spectral database (53,350 samples)

To further define the absolute reference stimuli used for training, the reflection spectra from each of the above sets was illuminated via one of four common indoor or outdoor cinema lighting sources, see Table 2. Again with all reflection spectra and all illuminants, training was performed with one permutation followed by performance verification with each of the other permutations.

Table 2. Scene illuminants considered in MPD design optimization

1) CIE Illuminant D65 2) CIE fluorescent, F2 3) CIE Illuminant A 4) Measured Hydrargyrum Medium-arc Iodide lamp (HMI)

The following indices were used to quantify observer metamerism magnitude and observer variability for both cost function minimization and subsequent performance verification. For observer metamerism, color difference formulae between two stimuli are used. For observer variability, three-dimensional CIELAB color error vectors are used. These indices are based on observer color-matching functions published from one of three previous studies. The first set is produced by Fedutina and Sarkar, et al. and represents a statistical compartmentalization of the original Stiles-Burch observer experiments (see Ref [6] – [8]). The second set represents a sampling of the CIE2006 model published by CIE TC1-36 for observer response as a function of age and field of view (see Ref [2]). The final set derives from Fairchild and Heckaman's work with Monte Carlo simulation of physiological transmission and absorption characteristics for the ocular media and $\bar{l}_\lambda$, $\bar{m}_\lambda$ and $\bar{s}_\lambda$ cones (see Ref [9]). Stimuli pairs input to the calculations derive from any established reference spectrum and a corresponding reproduction spectrum on the MPD.

$$\boldsymbol{OM_x = max(\overline{\Delta E_{y,P,i}})} \tag{2}$$

$$\boldsymbol{OM_{x,max} = max(\Delta E_{y,P,i})} \tag{3}$$

where $\mathbf{OM_x}$ refers to observer metamerism magnitude based on CMF sets from **x** = Sarkar/Fedutina, et al. (s), CIE2006 (c) or Heckaman/Fairchild (h). Color difference values between a reference stimuli and test sample are computed for **y** = ΔE_{ab} (ab), ΔE_{94} (94) or ΔE_{00} (00) for each patch in a patchset **P** for each observer **i** in the CMF set. The observer metamerism magnitude is the maximum individual observer average patchset color difference across all the patches in **P**. In this manner, the observer metamerism represents the on-average poorest color matching observer from the population of CMFs for the patchset. A slight variation of this metric, $\mathbf{OM_{x,max}}$ is based on measurement of the worst color difference patch across all observers in the given CMF set. This is thus the worst color match achieved across a full set of stimuli in the patchset considering all candidate observers. To minimize either of these metrics in a cost function suggests a move towards improving the color match between two stimuli for all observers in a population and thus a minimization of observer metamerism magnitude.

Observer variability metrics are summarized by equations 4 and 5.

$$\boldsymbol{OM_{x,var} = \overline{Vol(\Delta(L^*a^*b^*)_P)}} \tag{4}$$

$$\boldsymbol{OM_{x,varmax} = max(Vol(\Delta(L^*a^*b^*)_P))} \tag{5}$$

where $\mathbf{OM_{x,var}}$ refers to observer metamerism variability, the mean CIELAB ellipsoid volume constructed from CMF-based error vectors in L*, a* and b* from each patch in a patchset **P**. The metric is again dependent on the CMF set chosen as above. For the present work, covariance analysis is used to construct the ellipsoid volumes from individual observer CIELAB error vectors with a 90% statistical significance. $\mathbf{OM_{x,varmax}}$ is the maximum ellipsoid volume from all patches in the patchset and is thus the particular stimuli pair with the broadest observer variability.

The objective for the optimizations was to identify the most robust training spectra, illuminant and optimization parameters to develop an idealized MPD design with the most effective number of primaries across the larger set of validation stimuli. The primary spectra modeling progressed in two stages. In a first screening simulation, the NxP radiometric scaling matrix, **R**, necessary to generate spectral matches to the λxP training stimuli matrix, $\mathbf{S}_{\boldsymbol{train}}$, was computed via psuedoinverse linear algebra using equation 7. During optimization, λxN primary spectra, **PS**, were produced via iteration of the Gaussian transmission parameters, $\boldsymbol{\mu}$ and $\boldsymbol{\sigma}$, and using a concatenation of the resultant filter spectra in each channel with the projector illuminant spectra, $\boldsymbol{I}$, equation 6. Equation 8 was then used to predict the reconstructed spectral stimuli. The optimization was allowed to progress until a minimization of $\boldsymbol{OM_x}$ or $\boldsymbol{OM_{x,var}}$ was achieved for the original $\mathbf{S}_{\boldsymbol{train}}$ versus the reconstructed $\hat{\mathbf{S}}_{\boldsymbol{train}}$. Once primary spectra for each training scenario were determined, equations 7 and 8 were used to assess the **R** and $\hat{\mathbf{S}}$ matrices for the verification stimuli, $\mathbf{S}_{\mathbf{ver}}$. Observer metamerism metrics were again computed between $\hat{\mathbf{S}}_{\boldsymbol{ver}}$ and $\mathbf{S}_{\boldsymbol{ver}}$. For the second stage of simulation, **PS** spectra were retained from the screening models for each permutation. However, the **R** matrices in this variation were computed not via psuedoinversion of the spectral data but rather via a fully constrained nonlinear optimization, permitting much better spectral reconstructions to be produced though at the cost of computing speed.

$$\mathbf{PS} = \boldsymbol{diag}(\boldsymbol{I}) \cdot \mathbf{T} \tag{6}$$

$$\mathbf{R} = \boldsymbol{pinv}(\mathbf{PS}) \cdot \mathbf{S}_{\boldsymbol{patchset}} \tag{7}$$

$$\mathbf{PS} \cdot \mathbf{R} = \hat{\mathbf{S}}_{\boldsymbol{patchset}} \tag{8}$$

3. OPTIMIZATION RESULTS

Each of the first five patchsets from Table 1 were used independently to train the optimization of primary Gaussian parameters, followed by performance validation from each of the remaining sets and the SOCS set (which was itself not used as a trainer in the optimizing routines due to computational restrictions). To provide a clean baseline comparison, the patchsets were first illuminated by only a CIE D65 source to generate reference training stimuli and the Gaussian transmission filters iterated by the optimization routine were concatenated with only the xenon arc projector source to define **PS** (a contrast ratio of 10,000:1 was also used to set the MPD black). A starting guess of N=6 primaries with initial peaks, $\boldsymbol{\mu}$, distributed uniformly across the visible domain and with starting profile-widths, $\boldsymbol{\sigma}$, of 25nm was chosen. The optimization of the 12 Gaussian terms was performed via equations 7 and 8 to minimize $\boldsymbol{OM_s}$ (y= ΔE_{ab}) for the training spectra. Models from Ref [3] suggest optimizations incorporating $\boldsymbol{OM_c}$ or $\boldsymbol{OM_h}$ should deliver reasonably similar results. Constrained nonlinear optimization was used to restrict the peak filter transmission wavelengths to binned domains, each 50nm wide and distributed uniformly between 400 and 700nm. Transmission profile-widths were also constrained to a maximum upper bound. Table 3 summarizes the resultant Gaussian parameters for each of the six channels optimized in the five distinct training scenarios. The primaries synthesized from varying the training patchset are significantly different across each permutation of the above methodology, offering a fairly strong signal in the modeling. Figure 2 shows the observer metamerism and variability indices for the verified reproduction simulations for all of the patchsets as a function of each candidate training set.

Table 3. 6-channel Gaussian filter parameters optimized for each training patchset (D65 patch illumination, xenon projector source, minimization of OM_s)

Training Patches	Optimized Primary Gaussian Parameters μ/σ (nm)											
	1		2		3		4		5		6	
MacBeth 24	431	12.7	459	20.1	516	25.1	560	24.9	605	24.3	651	20.8
MacBeth DC	437	16.7	478	13.8	517	19.4	557	21.8	601	18.0	661	29.1
Kodak/AMPAS	436	14.8	472	12.9	518	19.5	559	22.4	606	18.5	650	17.3
Munsell	434	15.5	473	13.7	509	18.4	552	24.7	603	25.7	674	32.9
Big Metamers	436	14.0	470	14.2	522	21.1	570	22.7	621	17.2	670	14.6

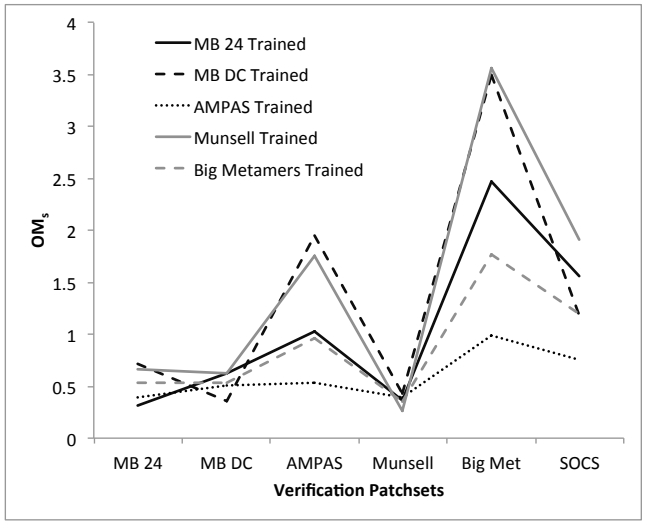

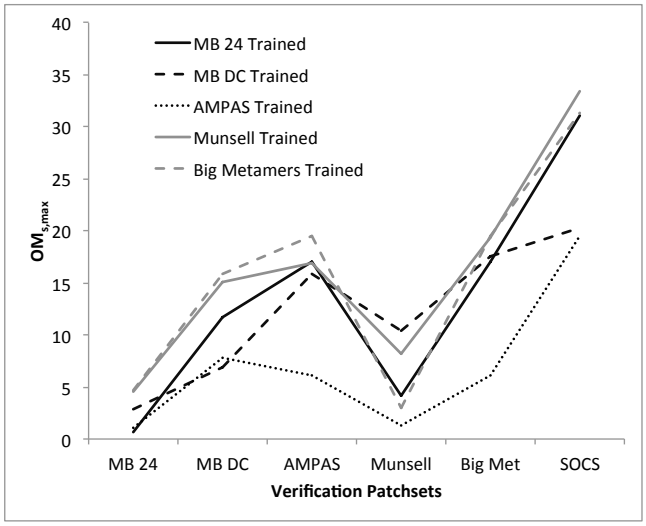

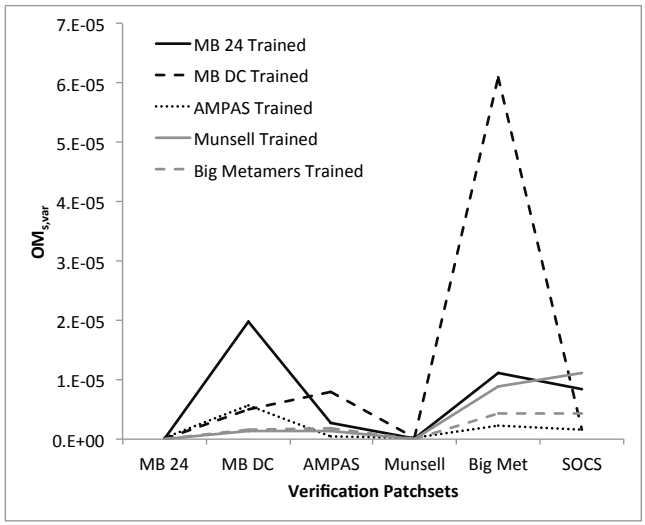

Figure 2. Psuedoinverse-optimized 6-channel MPD metamerism verifications derived from five candidate training spectra (D65 patch illumination, xenon projector source, minimization of OM_s); OM_s (upper left), $OM_{s,max}$ (upper right) & $OM_{s,var}$ (lower left)

The Kodak/AMPAS test spectra generate the most robust training results when all other patchsets are verified using its optimized primary spectra. This can be validated for both $\boldsymbol{OM_s}$ and $\boldsymbol{OM_{s,var}}$ indices and looking at all six of the verification patchsets. To prove the model is behaving as expected, Figure 2 shows that most verification patchsets perform best for average observer metamerism $\boldsymbol{OM_s}$ when trained by themselves while the AMPAS training is consistently second best for each. The lone exception is the Big Metamers set which introduces particularly difficult spectral reproduction objectives to the model. Here, the Kodak/AMPAS training set delivers better results than the self-trained scenario. For the large SOCS verification set, the Kodak/AMPAS trainer is clearly best in all three indices, followed by the Big Metamers and MacBeth DC trainers. Among the five candidate training sets, the Munsell and Macbeth DC patches perform most inconsistently across the full population of reference stimuli. Focusing on just verification results, it's interesting to note that each of the MacBeth patchsets and the Munsell spectra are all relatively insensitive to training permutations, suggesting they may be poor candidates for screening additional model variations going forward.

The first major variation from the above baseline scenario involves use of a constrained nonlinear optimization methodology for generating the radiometric scaling matrix, **R**, during prediction of $\hat{\mathbf{S}}_{ver}$ from each psuedoinverse-trained **PS**. Implementing this rigorous reconstruction, all trained primary variations prove much better at delivering reduced observer metamerism and variability across the verification patchsets, see Table 4. The AMPAS set still performs well but is effectively comparable to the other training permutations for $\boldsymbol{OM_s}$. Delving deeper into $\boldsymbol{OM_{s,max}}$ values across all permutations, however, the AMPAS set maintains reasonable superiority along with the MacBeth DC set. Nonlinear optimization of **R** generates excellent spectral reproductions of the verification patches regardless of optimized MPD primary set but at the cost of greatly increased computation time. In fact, Munsell and SOCS verifications were omitted from this analysis due to excessive processing requirements for the 1,300 and 50,000 patches in each, respectively.

Table 4. Nonlinear-optimized 6-channel MPD metamerism verifications derived from five candidate training spectra (D65 patch illumination, xenon projector source, minimization of $\boldsymbol{OM_s}$)

Training Patchset	Observer Metamerism, OM_s				Max Observer Metamerism, $OM_{s,max}$			
	MB 24	**MB DC**	**AMPAS**	**Big Met**	**MB 24**	**MB DC**	**AMPAS**	**Big Met**
MacBeth 24	0.14	0.16	0.15	0.32	0.43	4.24	1.36	3.46
MacBeth DC	0.08	0.08	0.10	0.12	0.15	0.18	1.23	0.63
Kodak/AMPAS	0.12	0.13	0.13	0.19	0.30	0.64	0.87	0.79
Munsell	0.07	0.07	0.08	0.13	0.25	2.17	0.70	1.48
Big Metamers	0.30	0.35	0.32	0.41	0.71	1.03	0.89	2.42

Varying starting guesses for the $\boldsymbol{\mu}$ and $\boldsymbol{\sigma}$ Gaussian parameters in each channel makes very little difference in results as long as the peak wavelengths are well distributed throughout the 400-700nm domain. A small improvement is seen, though, when the iterating peak wavelengths are permitted to vary subject to a monotonic vectorization versus each primary being binned in a restricted spectral span. The latter technique was hypothesized to be beneficial to enforcing full spectrum coverage across all visible wavelengths in the design though proved somewhat restrictive to the observer metamerism objective function. Figure 3 shows the training quality when the six transmission peaks are permitted to iterate in a monotonic series to any wavelengths between 400 and 700nm. Only the MacBeth Color Checker training is hampered versus the original compartmentalization strategy. For a sense of scale, the average $\boldsymbol{OM_s}$ across all six verification sets produced via the Kodak/AMPAS training drops from 0.59 when primary peaks are binned to 0.47 when non-binned. Also shown are the resultant peak wavelengths and profile-widths for the Kodak/AMPAS training permutation, comparing the original binned result to the non-binned result. The spectra do change somewhat significantly with non-binned primaries #5 and #6 optimizing to positions that would have been prohibited in the binned permutation.

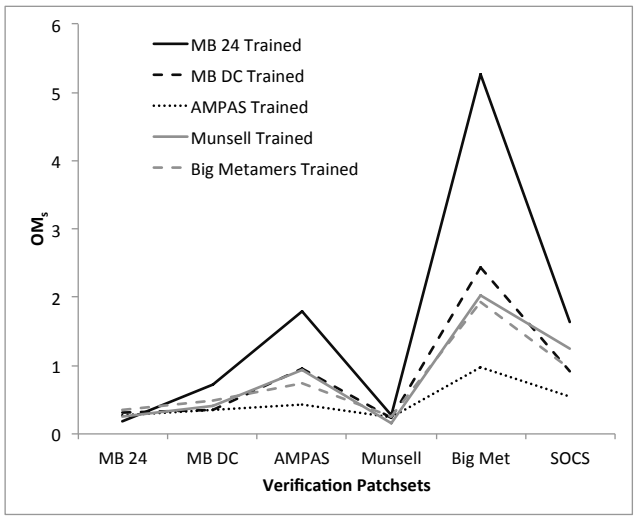

Primary	Binned	Non-binned
1	μ = 436 σ = 14.8	426 10.4
2	472 12.9	456 17.7
3	518 19.5	509 19.6
4	559 22.4	551 23.1
5	606 18.5	599 19.4
6	650 17.3	643 18.3

Figure 3. Psuedoinverse-optimized 6-channel MPD metamerism performance derived from five candidate training spectra with primary peaks permitted to optimize to any wavelength between 400 and 700nm (D65 patch illumination, xenon projector source, minimization of $\boldsymbol{OM_s}$); resultant Gaussian parameters for the binned and non-binned optimizations

Relative to the number of primaries necessary to produce optimum metamerism reduction, $N = 7$ and 8 were shown to generate some performance benefits versus systems with 6 or fewer total primaries. Figure 4 summarizes trends in observer metamerism and variability as a function of primary count for the Kodak/AMPAS verification set when trained by itself. While $\boldsymbol{OM_s}$ and $\boldsymbol{OM_{s,var}}$ see diminishing incremental improvements above 5 primaries, $\boldsymbol{OM_{s,max}}$ experiences a notable jump with an 8th primary added.

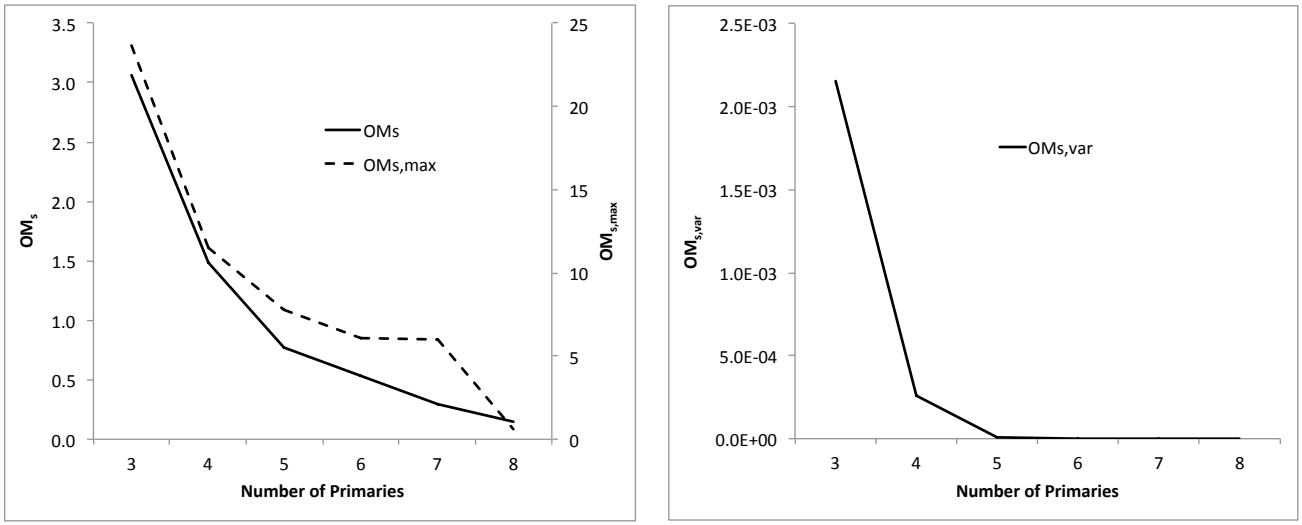

Figure 4. Psuedoinverse-optimized MPD metamerism performance as a function of modeled primary count (training via Kodak/AMPAS set, D65 patch illumination, xenon projector source, minimization of $\boldsymbol{OM_s}$)

Simulations to this point have restricted the reference stimuli to D65 illumination. To understand implications for other common light sources in photographic applications, the baseline analysis was repeated with each of the other three sources used for training. The only major differences versus the baseline results of Figure 2 were inclusion of 8

primaries in the optimized design and verification spectra inclusive of all six patchsets under all four illuminants. $\boldsymbol{OM_s}$ results for the Kodak/AMPAS and SOCS verification sets when trained using the Kodak/AMPAS patches under each of the four illuminants in Table 2, respectively, are summarized in Figure 5. Additionally, training was attempted with a Kodak/AMPAS set illuminated by all four illuminants simultaneously (thus comprising 760 unique stimuli). Verification scenarios are shown for these two patchsets under each Table 2 illuminant individually along the x-axes. A few notable trends in the MPD designs are evident. First, for each verification illuminant, the best training comes from a matched training illuminant. The HMI-illuminated verification set is best when HMI is similarly used for training, for example. Overall, the HMI training yields the best results in verification when averaged across all verification illuminants. The CIE F2 illuminant, on the other hand, is the poorest trainer of the set. Interestingly, the D65 trainer is also quite poor for generating HMI and F2-based verifications. For training F2-illuminated verifications, only the F2 trainer is adequate as each of the other three training illuminants are quite poor. The F2 spectra is significantly less continuous across the visible spectrum versus the other three, which may explain this performance, see Figure 6. Finally, the compromised trainer, inclusive of all four illuminants and the Kodak/AMPAS patches, does a solid job for all four verification scenarios for both of these patchsets.

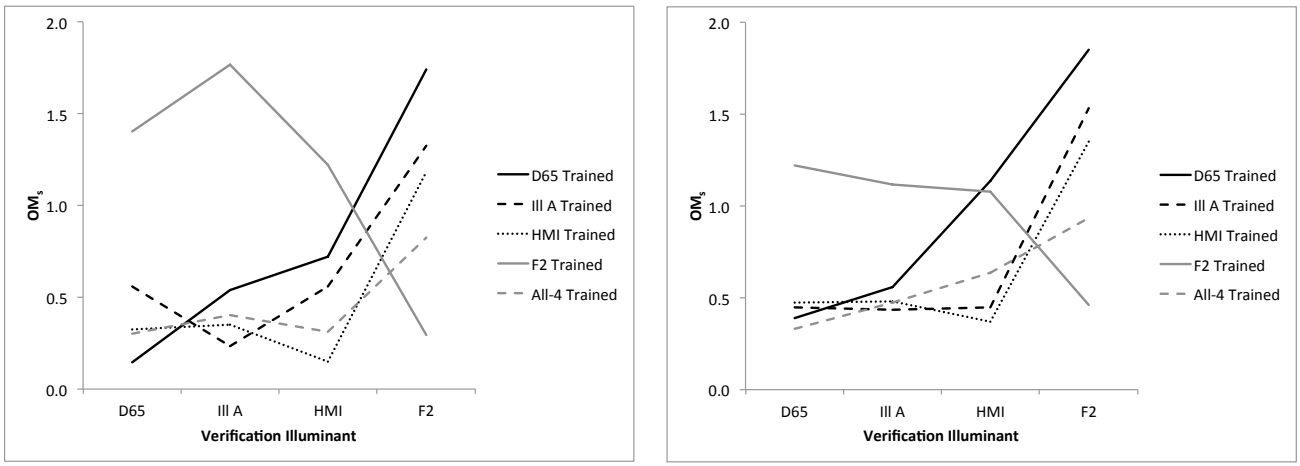

Figure 5. Psuedoinverse-optimized 8-channel MPD metamerism verifications as a function of training illuminant (training via Kodak/AMPAS set, xenon projector source, minimization of $\boldsymbol{OM_s}$); Kodak/AMPAS verification results (left) vs SOCS verification results (right)

3. MPD PROTOTYPE

The initial RIT MPD prototype was simulated based on results from the previous optimization studies, focusing specifically on the key learnings gained from investigating the various training permutations. The model incorporated 8 primaries iterated to minimize $\boldsymbol{OM_s}$ based on psuedoinversion training inclusive of the Kodak/AMPAS patchset and the "All-4" illumination spectra. Primary peak wavelengths were non-binned. One practical modification versus the previous models came in the form of the projector illumination source implemented. Consumer-grade Optoma DX339 projectors were identified to construct a first prototype system, each using a UHP lamp with the spectra shown in Figure 1. Further, the contrast of these projectors was roughly 2,000:1 rather than the 10,000:1 xenon arc source previously modeled. The Optoma DX339 projector is a time-multiplexed, single-chip DLP system which uses a spinning filter wheel with 6 color segments to generate reproduction of RGB video signals. For incorporation into the RIT MPD, the filter wheels were removed permitting a monochromatic modulation of the lamp spectra within the full resolution of the DLP chip (1024x768). To avoid impact from any internal color processing, signals sent to the projector were restricted to neutral scale values in 8-bit with all three color channels equivalent. The projector electro-optic transfer functions were also extensively characterized to permit absolute radiometric modeling.

Figure 7 summarizes the best simulated Gaussian primaries for an $N = 8$ design cascaded with the source spectrum of the consumer UHP lamp. The resulting primary transmission filters are relatively narrow-band and so the change in projector illumination source from xenon to UHP for the actual prototype design yielded only minor observer metamerism performance penalties. As example for the Kodak/AMPAS verification set, $\boldsymbol{OM_s}$ actually improved very slightly with verification illuminants of D65 and Ill A while yielding a result nearly 100% poorer for the F2 verification. For the SOCS set, $\boldsymbol{OM_s}$ was 20% poorer for D65, IllA and HMI and 100% poorer for F2.

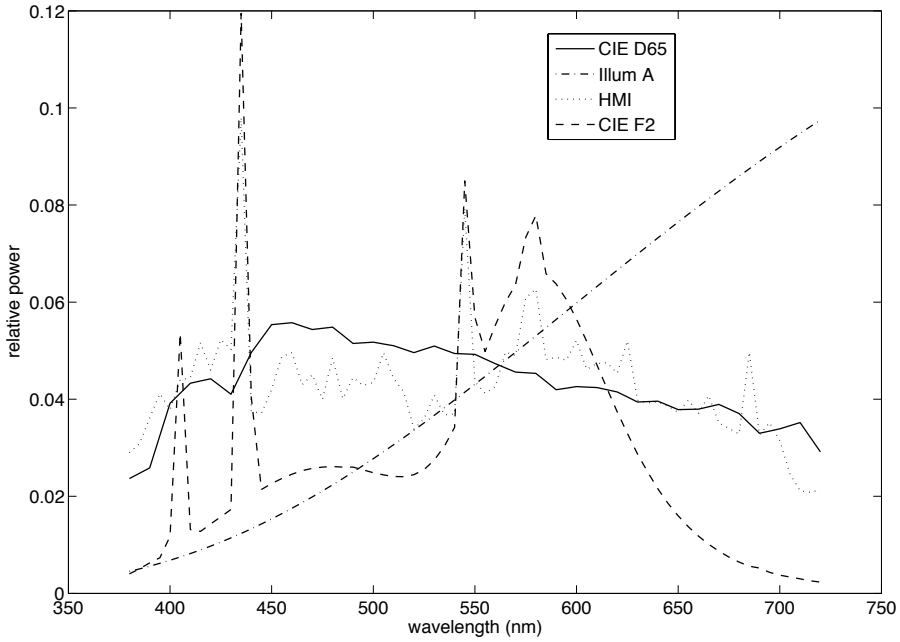

Figure 6. MPD training illuminant spectra

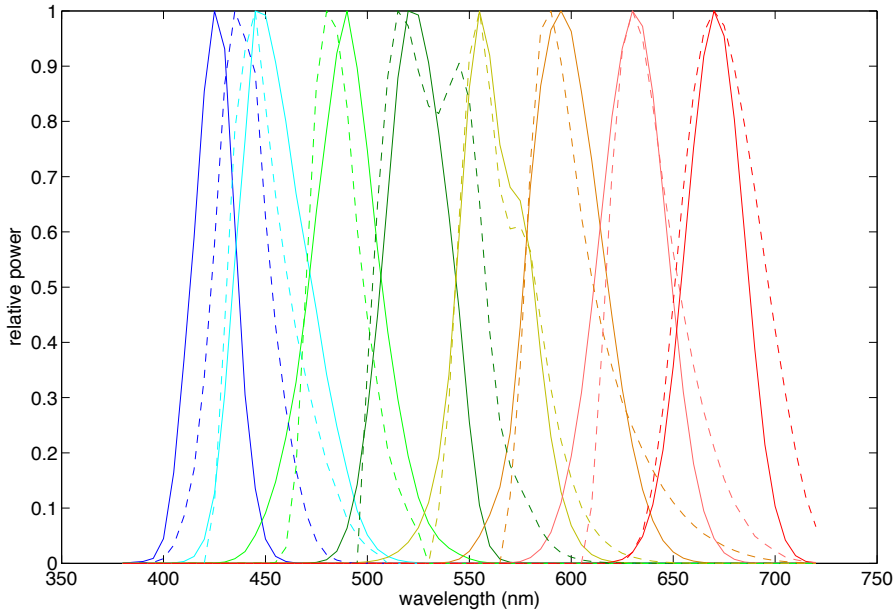

Figure 7. Optimized UHP-concatenated 8-channel primaries from Gaussian model (solid) versus primaries simulated from commercially available color filters (dashed) for RIT MPD

Ultimately, Gaussian transmission filters which perfectly match the optimization results of Figure 7 do not exist and a compromised set built from commercially available materials was chosen instead. In Figure 7 are shown modeled primaries utilizing color filters closest in performance to the Gaussian predictions. These selections followed an exhaustive search of materials available from major manufacturers. The penalty for choosing from only currently available filters is significant. Verification simulations for the real filters yielded $\boldsymbol{OM_s}$ values approximately 8x worse than the ideal case across all of the previously tabulated patchsets and illuminants. Average $\boldsymbol{OM_{s,max}}$ suffered a penalty of approximately 3x and average $\boldsymbol{OM_{s,var}}$ was twice the Gaussian model optimum. Clearly, a commissioned set of filters produced for subsequent prototypes would serve to radically improve the expected performance of the constructed system. At the same time, these metamerism assessments are reflective of the psuedoinverse color reproduction strategy of equations 7 and 8 only. Additional experimentation with the RIT MPD will take advantage of further refinements to stimuli matches such as nonlinear optimization of radiometric scalars, **R**, or paramer correction of reproductions to generate standard colorimetric matches to example reference stimuli such as in Ref [3].

The prototype RIT MPD was constructed from individual Optoma projectors all modified to remove their color filter wheels and retrofitted with the individually chosen external filters. Optical paths were overlaid to a single screen, permitting reconstruction of additive multispectral images. Each projector was treated as a single, independent color channel driven via independent NVIDIA GeForce GT120 graphics cards from a modified Mac Pro. Custom software was written to perform optical alignments and drive full resolution multispectral images to all color channels. Installation and subsequent characterization of the 8-channel system yielded some spectral fluctuation versus the Figure 7 models. Most was due to variability in UHP lamp spectra amongst the 8 projectors, though some units also suffered from significant temporal drift. Upon implementation of temperature control equipment and improved spectral stability, an alternate configuration comprising only 7 primaries was ultimately deemed best for laboratory experiments. Metamerism performance proved effectively equivalent to the 8-channel simulation; the measured spectra for this system is shown in Figure 8. The gamut of the MPD in u'v' coordinates versus standard colorspaces ITU-R Rec. 709, ITU-R-Rec. 2020 and SMPTE 431 is shown in Figure 9. Gamut area dvantages versus even the monochromatic UHDTV performance specifications of Rec. 2020 are evident. Ref [3] offers significant analysis of the RIT MPD's modeled improvements in observer metamerism and variability versus several representative RGB displays. Further, experiments are currently underway with observers to confirm the advantage of the 7-channel system versus contemporary displays (including laser systems) in minimizing observer variability when generating matches to reference spectra. These experiments are intended to validate the utility of both the color vision models employed and the metamerism and variability indices suggested in this work.

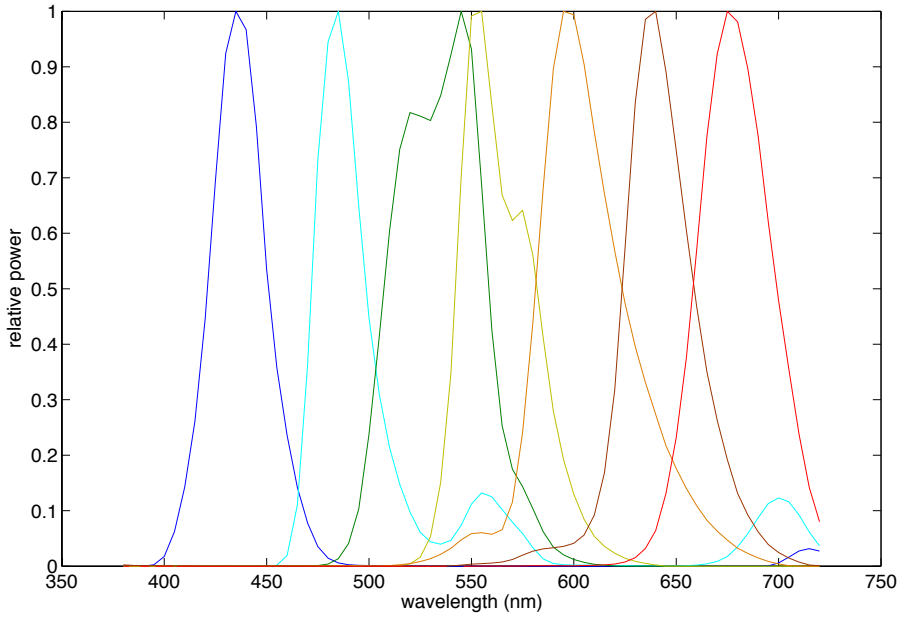

Figure 8. Measured primaries for constructed 7-channel RIT MPD

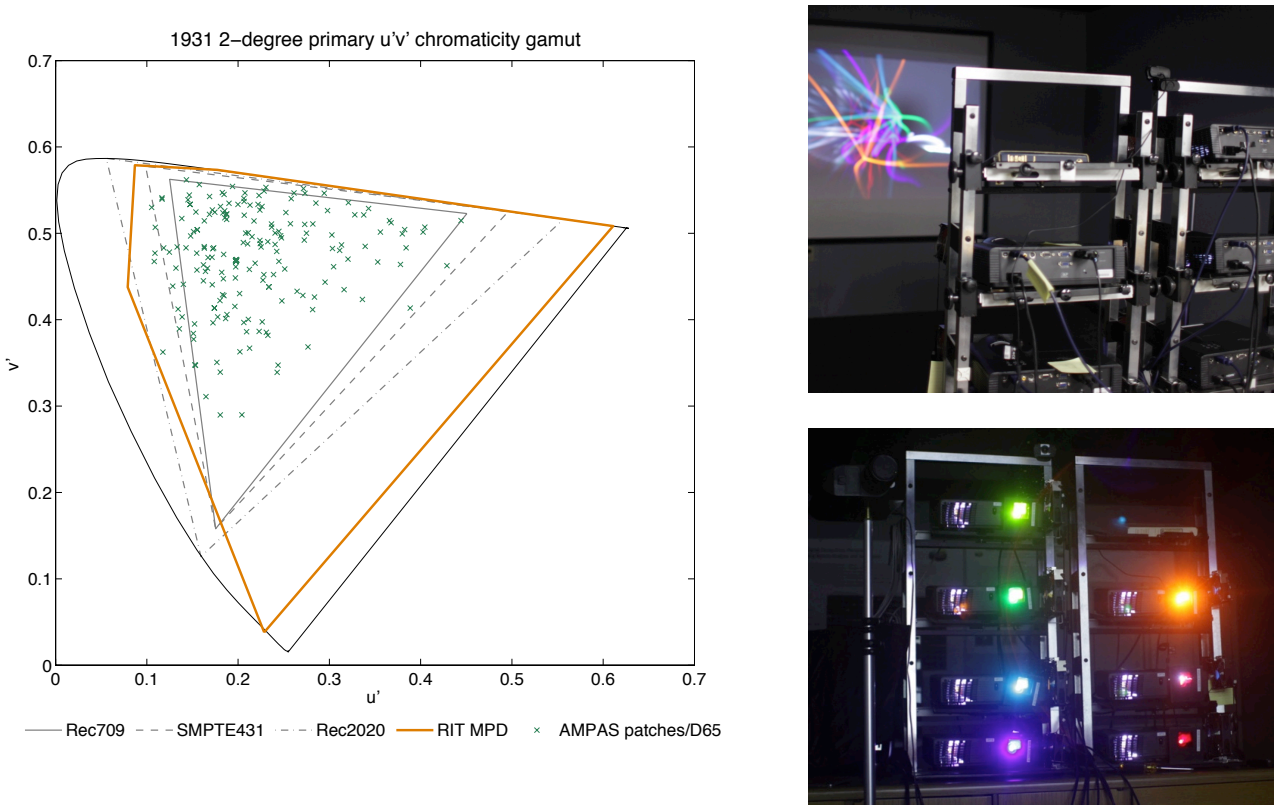

Figure 9. RIT 7-channel projector chromaticity gamut - color points representing Kodak/AMPAS color patches illuminated by CIE D65 shown for reference; also included are images of the physical form factor of the prototype MPD

3. CONCLUSIONS

Emission spectra for the different color channels of a multiprimary display can be optimized to reduce observer metamerism and variability. An investigation of training permutations focusing on different metamerism indices, reference spectral stimuli (illuminants and reflective patches), primary counts, color filter bandpass constraints and projection illuminants delivered a prototype MPD design which was ultimately constructed for use in visual experiments. Remaining challenges include engineering strong spectral stability over time domains minimally acceptable for the intended uses of the system. In addition to the 7-projector unit described, a second form factor has been built with a single projector and 7 optically-isolated primary channels recombined in an integrating chamber for delivering a single area of uniform spectral intensity to an observer. This unit presents advantages in spectral and radiometric stability over extensive time periods and through multiple system power cycles but sacrifices capability to render actual images from multispectral content. The spectra of the primaries in this color patch generator are effectively identical to those shown in Figures 8 and 9. Future work with both systems will serve to validate the RIT MPD's benefits in metamerism reduction amongst color-normal observers when compared to traditional small-gamut and large-gamut RGB displays and is intended as empirical confirmation of modeled results published in Ref [3].

REFERENCES

[1] Berns, R. S., "Principles of Color Technology, 3rd ed.," John Wiley & Sons, New York, 49-56 (2000)

[2] CIE, "Fundamental chromaticity diagram with physiological axes – part 1," CIE Pub. 170-1:2006 (2006)

[3] Long, D. and Fairchild, M. D., "Modeling observer variability and metamerism failure in electronic color displays," J. Imaging Science and Technology 58(3), (2014)

[4] Sony Corporation White Paper, "Colour matching between OLED and CRT," v1.0, (Feb 15, 2013)

[5] Donato, M. and Long, D., "Towards standardizing a reference white chromaticity for HDTV," progress report to SMPTE ST/RP 2080 committee on measurement and calibration procedures for HDTV displays, (Nov 18, 2014)

[6] Sarkar, A., Blonde, L., Le Callet, P., Autrusseau, F., Morvan, P. and Stauder, J., "Toward reducing observer metamerism in industrial applications: colorimetric observer categories and observer classification," Proc. CIC18, (2010)

[7] Sarkar, A., Autrusseau, F., Vienot, F., LeCallet, P. and Blonde, L., "From CIE2006 model to improved age-dependent and average colorimetric observers," JOSA 28(10), (2011)

[8] Fedutina, M., Sarkar, A., Urban, P. and Moran, P., "(How) Do observer categories based on color matching functions affect the perception of small color differences?" Proc. CIC19, (2011)

[9] Fairchild, M. D. and Heckaman, R. L., "Metameric observers: a Monte Carlo approach," Proc. CIC21, (2013)

[10] Kohonen, O., Parkkinen, J. and Jaaskelainen, T., "Databases for spectral color science," CR&A 31(5), 381-388 (2006)

[11] Tajima, J., "Development and analysis of Standard Object Colour Spectra Database (SOCS)," Proc. Multispectral Imaging and Color Reproduction, Chiba, Japan, 26-33 (1999)